

**A STEP TOWARDS A REDUCED ORDER MODELLING OF FLOW CHARACTERIZED  
BY WAKES USING PROPER ORTHOGONAL DECOMPOSITION**

**Eivind Fonn**

CSE Group  
Mathematics and Cybernetics  
Sintef Digital  
7034, Trondheim, Norway  
Email: eivind.fonn@sintef.no

**Adil Rasheed \***

CSE Group  
Mathematics and Cybernetics  
Sintef Digital  
7034, Trondheim, Norway  
Email: adil.rasheed@sintef.no

**Mandar Tabib**

CSE Group  
Mathematics and Cybernetics  
Sintef Digital  
7034, Trondheim, Norway  
Email: mandar.tabib@sintef.no

**Trond Kvamsdal**

Department of Mathematical Sciences  
NTNU  
Alfred Getz vei 1  
7491, Trondheim, Norway  
Email: trond.kvamsdal@math.ntnu.no

**ABSTRACT**

*High fidelity simulations of flow might be quite demanding, because they involve up to  $O(10^6 - 10^9)$  degrees of freedom and several hours (or even days) of computational time, also on powerful hardware parallel architectures. Thus, high-fidelity techniques can become prohibitive when we expect them to deal quickly and efficiently with the repetitive solution of partial differential equations. One set of partial differential equation that we encounter on a regular basis is the Navier Stokes Equation which is used to simulate flow around complex geometries like sub-sea structures. To address the issues associated with computational efficiency, a field of Reduced Order Modelling is evolving fast. In this paper we investigate Proper Orthogonal Decomposition as a potential method for constructing reduced bases for Reduced Order Models. In the case of flows around cylindrical bodies we found that only a few modes were sufficient to represent the dominant flow structures and energies associated with them making POD to be an attractive candidate for bases*

*construction.*

**INTRODUCTION**

Numerical methods and tools to simulate flow around complex geometries like wind turbines and subsea structures have evolved a lot in recent years. However, their usage requires access to high performance computing facilities, which are not always possible. Additionally, there has been an ever-increasing demand of computationally efficient desktop tools that can be used for design and real time control and management systems. These requirements are diametrically opposite to what we can achieve through the large array of high fidelity simulation tools available at our disposal. For flow simulations, the governing equations are Navier Stokes Equation written in terms of certain input parameters whose effect one might want to investigate. For this kind of problems, Reduced Order Modeling (ROM) is a generic expression used to identify any approach aimed at replacing the high fidelity problem by one featuring a much lower numerical complexity. Being able to evaluate the solution of this

---

\*Address all correspondence to this author.

latter problem, for any new parameter instance, at a cost that is independent of the dimension of the original high-fidelity problem, is the key to success of any reduced order model. Reduced-Basis (RB) methods represent a remarkable instance of ROM techniques ([1]). They exploit the parametric dependence of the PDE solution by combining a handful of high fidelity simulations (or snapshots) computed a priori for a small set of parameter values. By this approach, a very large algebraic system is replaced by a much smaller one, whose dimension is related to the number of snapshots. The key is then to construct the reduced bases to be used in ROM. One method that can be used for constructing such bases and we have investigated here is called the Proper Orthogonal Decomposition (POD). The workflow requires different modules which are described below:

1. High fidelity simulation module: This module is used for conducting high fidelity simulations of flows around sub-sea structures (cylinder in this case but not limited to it) for varying inlet boundary conditions (uniform or pulsating inflows). The solver is based on the OpenFoam (OF) framework.
2. Data storage and processing module: High fidelity simulation results also called snapshots are huge in size and requires efficient storage and processing. The high fidelity simulation results, generally conducted on unstructured meshes in VTK format are first interpolated on structured meshes. These are then converted to HDF5 or NETCDF4 formats and are made available via an OpenDAP server. Doing so obviates the need to duplicate data on multiple computers for further processing.
3. Reduced bases construction module: This module consists of routines for conducting POD to construct the reduced bases.

## MODULE DESCRIPTION

A more technical description of the modules is provided in the following subsections.

### HIGH FIDELITY SIMULATION MODULE

A transient 3D computational fluid dynamics (CFD) model is utilized. The model computes velocity, pressure and turbulence fields. The turbulence is modeled using a one-equation sub-grid scale (SGS) turbulent kinetic energy LES model. The equations for LES are derived by applying filtering operator to the Navier-Stokes equations. The filtering results in Eqn. (1) and (2).

$$\frac{\partial \bar{u}_i}{\partial t} = 0 \quad (1)$$

$$\frac{\partial \bar{u}_i}{\partial t} + \frac{\partial}{\partial x_j} (\bar{u}_i \bar{u}_j) = -\frac{\partial \bar{p}}{\partial x_i} - \frac{\partial B_{ij}}{\partial x_j} + \nu \frac{\partial^2 \bar{u}_i}{\partial x_j \partial x_j} \quad (2)$$

where  $\bar{u}_i$  is the filtered (or resolved) velocity,  $\bar{p}$  the filtered pressure,  $\nu$  the dynamic viscosity and

$$B_{ij} = \overline{u_i u_j} - \bar{u}_i \bar{u}_j \quad (3)$$

The term  $\mathbf{B}$  can be modeled using Eqn. 4

$$\mathbf{B} = \frac{1}{3} \text{Tr}(\mathbf{B}) \mathbf{I} + \nu_{sgs} (\nabla \mathbf{u} + \nabla T \mathbf{u}) \quad (4)$$

where  $T(\mathbf{B})$  stands for the trace of the tensor  $\mathbf{B}$ ,  $\mathbf{I}$  is the identity matrix, and  $\nu_{sgs}$  is the so called SGS viscosity which is expressed in terms of the subgrid turbulent kinetic energy  $k_{sgs}$  using Eqn. (5).

$$\nu_{sgs} = (C_k \Delta) k_{sgs}^{1/2} \quad (5)$$

where  $C_k = 0.094$ .  $k_{sgs}$  is computed using its transport Eqn. (6).

$$\begin{aligned} \frac{\partial k_{sgs}}{\partial t} + \frac{\partial \bar{u}_i k_{sgs}}{\partial x_i} = & 2\nu_{sgs} |\bar{D}_{ij}|^2 - C_e \frac{k_{sgs}^{3/2}}{\Delta} \\ & + \frac{\partial}{\partial x_i} \left( \nu_{sgs} \frac{\partial k_{sgs}}{\partial x_i} \right) + \nu \frac{\partial^2 k_{sgs}}{\partial x_i \partial x_i} \end{aligned} \quad (6)$$

where  $\bar{D}_{ij}$  is the filtered rate of strain tensor, and  $C_e = 1.048$  is a constant.

To ensure continuity, an elliptic equation for the modified pressure is created by combining continuity equation with divergence of momentum equation. This elliptic equation along with the momentum equation and sub-grid scale turbulent kinetic energy equation are solved in a segregated manner using the PISO-SIMPLE algorithm (PIMPLE algorithm). The algorithm ensures use of a higher time step for transient simulations. The OF uses a finite volume discretization technique, wherein all the equations are integrated over control volumes (CV) using Green Gauss divergence theorem. The Gauss divergence theorem converts the volume integral of divergence of a variable into a surface integral of the variable over faces comprising the CV. Thus, the divergence term defining the convection terms can simply be computed using the face values of variables in the CV. The face values of variables are obtained from their neighboring cell centered values by using a convective scheme. In this work, all the equations (except  $k_{sgs}$ ) use second order linear discretization scheme, while the turbulent equations use a blend of

linear-upwind convection schemes. Similarly, the diffusion term involving Laplacian operator (the divergence of the gradient) is simplified to computing the gradient of the variable at the face. The gradient term can be split into contribution from the orthogonal part and the non-orthogonal parts, and both these contributions have been accounted for. This module has been used in the past to simulate flow in complex terrain (see [2], [3], [4]), flow around rotating turbines ([5]) within our FSI-WT project ([6]).

## DATA STORAGE AND PROCESSING MODULE

For processing the potentially large amounts of data from the high fidelity simulations, it is desirable to achieve a networked workflow. This should minimize the strain on the local disk, as well as duplication of effort among users.

To this end, an OPeNDAP server was set up. OPeNDAP (“Open-source Project for a Network Data Access Protocol”) is a data transport protocol based on HTTP (Hyper Text Transfer Protocol), allowing a central server to serve common data storage formats (for example NetCDF4, HDF5), so that clients can read only what they need and when they need it. As long as the client-side accessing library is well written, for the end user this should be functionally identical to reading local files.

No support is available for serving VTK files in this manner. However, since OPeNDAP is built on HTTP, it ignores files which it does not understand, VTK among them. This makes it possible to write a “naive” wrapper for VTK, which downloads the complete data of the file to a temporary location and opens it instead.

## REDUCED BASES CONSTRUCTION MODULE

Given an ensemble of solutions to a problem  $\{\varphi_i\}_{i=1}^p$  (evaluated at different timesteps, say), each adjusted to have mean zero, we seek a set of orthogonal modes  $\{\zeta_j\}_{j=1}^p$  such that the reconstructed ensemble

$$\varphi_i^N = \sum_{j=1}^N a_i^j \zeta_j$$

truncated at order  $N$  can represent to some reasonable degree the original ensemble. Assuming also that the original ensemble represents a “typical” set of solutions to the given problem, one might hope that  $\{\zeta_j\}_{j=1}^N$  gives an appropriate basis and function space for the sparse representation of such solutions.

The method of principal orthogonal decomposition (POD) provides a well tested mechanism for this. The closeness of approximation should be measured in some norm  $\|\cdot\|_a$ , and the square of this norm corresponds to the statistical notion of variance. The inner product  $\langle \cdot, \cdot \rangle_a$  that induces the norm corresponds

to covariance. The covariance matrix is then

$$C_{ij} = \frac{1}{N} \langle \varphi_i, \varphi_j \rangle_a.$$

Its eigenpairs  $(\mathbf{q}_i, \lambda_i)$  give the modes  $\zeta_i$  according to

$$\zeta_i = \frac{1}{\sqrt{\lambda_i}} \sum_j \mathbf{q}_i^j \varphi_j.$$

It can be seen that if the eigenvectors  $\mathbf{q}_i$  of  $\mathbf{C}$  are chosen to be orthonormal, i.e.  $\mathbf{q}_i^T \mathbf{q}_j = \delta_{ij}$ , then  $\zeta_i$  are orthonormal in the  $a$ -inner product, viz.

$$\langle \zeta_i, \zeta_j \rangle_a = \frac{1}{\sqrt{\lambda_i \lambda_j}} \mathbf{q}_i^T \mathbf{C} \mathbf{q}_j = \sqrt{\frac{\lambda_j}{\lambda_i}} \delta_{ij} = \delta_{ij}.$$

The sum of eigenvalues is equal to the trace of  $\mathbf{C}$ , and thus can be interpreted as the average variance in the ensemble. In particular, each individual eigenvalue  $\lambda_i$  is equal to the average variance captured by its corresponding mode throughout the ensemble. Therefore the truncation order  $N$  should be chosen such that

$$\frac{\sum_{i=N+1}^p \lambda_i}{\sum_{i=1}^p \lambda_i} \leq \varepsilon$$

for some predetermined level of tolerance  $\varepsilon$ , and it is hoped that suitably low  $\varepsilon$  still yield  $N$  such that  $N(\varepsilon) \ll p$ . In the remainder of this work we have chosen to focus on the representation of *velocity*. Thus the covariance function can be written

$$\langle (\bar{\mathbf{u}}_i, p_i), (\bar{\mathbf{u}}_j, p_j) \rangle_a = \int_{\Omega} \bar{\mathbf{u}}_i \cdot \bar{\mathbf{u}}_j,$$

Where a solution  $\varphi_i$  in this case has been identified with its velocity and pressure solutions  $\mathbf{v}_i$  and  $p_i$ . A more appropriate choice for representing both velocity *and* pressure are covariance functions of the form

$$\langle (\bar{\mathbf{u}}_i, p_i), (\bar{\mathbf{u}}_j, p_j) \rangle_a = \int_{\Omega} (\bar{\mathbf{u}}_i \cdot \bar{\mathbf{u}}_j + c p_i p_j),$$

where an appropriate scaling constant  $c$  must be chosen to make the two quantities comparable, e.g.

$$c = \frac{\sum_i \|\bar{\mathbf{u}}_i\|^2}{\sum_i \|p_i\|^2}.$$

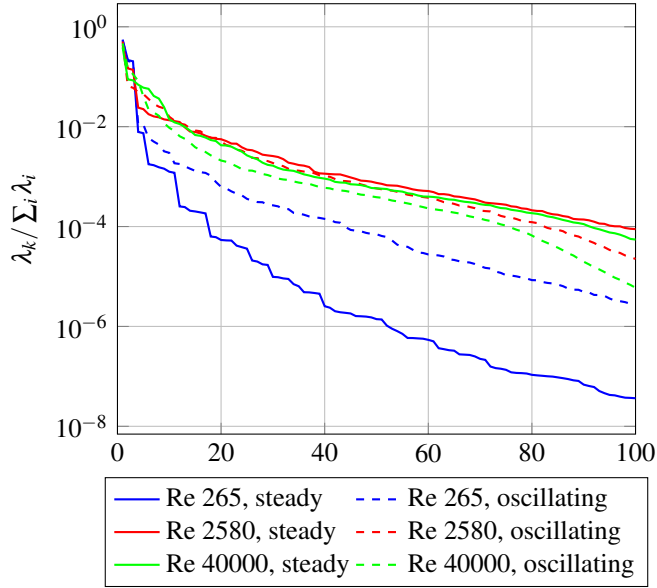


**FIGURE 1.** ENERGY SPECTRA OF ALL SIX CASES UP TO 100 EIGENVALUES.

### SNAPSHOT GENERATION

To generate snapshots, LES simulations of flow around a circular cylinder was conducted at three different Reynolds number ( $Re$  based on cylinder diameter and bulk inlet velocity) of  $Re = 265$ ,  $Re = 2580$  and  $Re = 40000$ . In addition to three simulations with uniform inlet velocity, three simulations with pulsating inflow boundary conditions were also conducted. The diameter ( $D$ ) of cylinder is  $1 m$ . The bulk or free-stream inlet velocity ( $U_\infty$ ) is  $1 m/s$  for uniform inflow case. Pulsating inflow was provided using equation 7 below.

$$U(t) = U_\infty + \Delta U \sin(2\Pi ft) \quad (7)$$

As per suggestion by [7], the values of  $\Delta U$  and  $f$  are selected so that the parameter  $\varepsilon = \frac{\Delta U}{2\Pi f D}$  is around 0.2. This ensures a sufficiently large threshold window for lock-on to occur [8]. The Reynolds number is varied by varying the fluid viscosity. These three Reynolds numbers represent different physical regimes. Figure 2 shows the computational domain used in the simulations. The domain size is  $40D \times 20D \times 1D$  in the streamwise ( $X$ ), flow normal ( $Y$ ) and spanwise ( $Z$ ) directions. Periodic boundary condition is applied in the spanwise directions while a slip boundary condition is applied in the flow-normal direction. The inlet (on left) and outlet (on right) boundaries are specified along streamwise direction. The cylinder is placed such that its centre is about  $10D$  from the inlet plane and the outlet plane is located about  $30D$  downstream from the cylinder centre. For  $Re = 2580$  and  $Re = 40000$ , hexahedral dominated mesh size is about 7.2

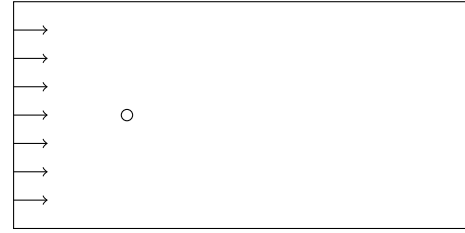


**FIGURE 2.** DOMAIN SKETCH.

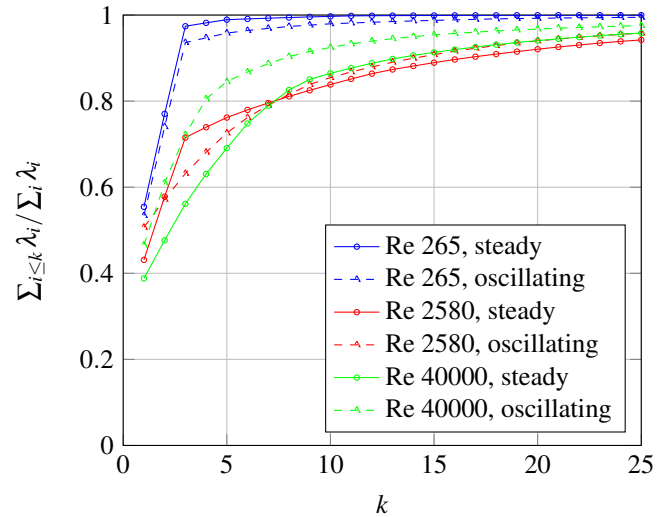


**FIGURE 3.** CUMULATIVE ENERGY SPECTRA OF ALL SIX CASES UP TO 25 EIGENVALUES.

million cells, with region around cylinder and downstream of vortex shedding path being highly refined. The mesh element size ranges from  $0.003D$  close to the cylinder surface (resulting in  $y^+ < 1$ ) to  $0.5D$  furthest away from the cylinder surface in the computational domain. Details on domain set up, mesh resolution, boundary conditions and physical interpretation of results can be found in [8]. More details regarding the physical interpretation of the results can be found in [7] and [9]. We have intentionally omitted similar discussion here since, our objective in this paper is to just evaluate the applicability of ROM using POD.

### RESULTS AND DISCUSSIONS

The data for each simulation, representing in each case at least one principal period, sampled at 20Hz, was interpolated on a uniform rectilinear grid measuring  $400 \times 200$  elements, with a gridsize of  $0.1D$ .

The results regarding the energy spectra can be observed in Fig. 1 and Fig. 3. In all cases, about 30 modes suffice to cover

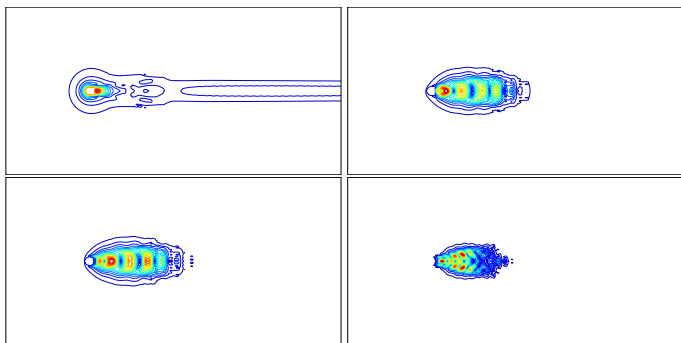


**FIGURE 4.** FIRST FOUR MODES OF THE STEADY 265 REYNOLD'S NUMBER CASE.

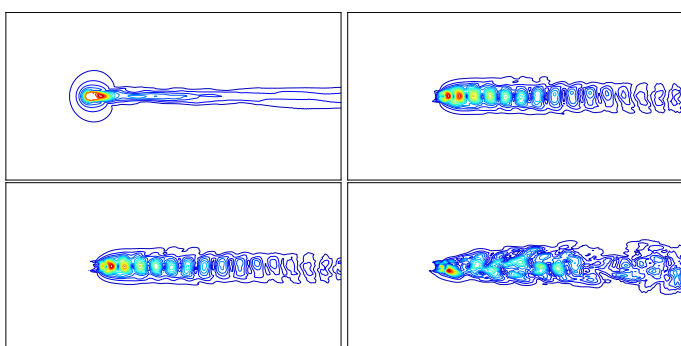


**FIGURE 5.** FIRST FOUR MODES OF THE STEADY 2580 REYNOLD'S NUMBER CASE.

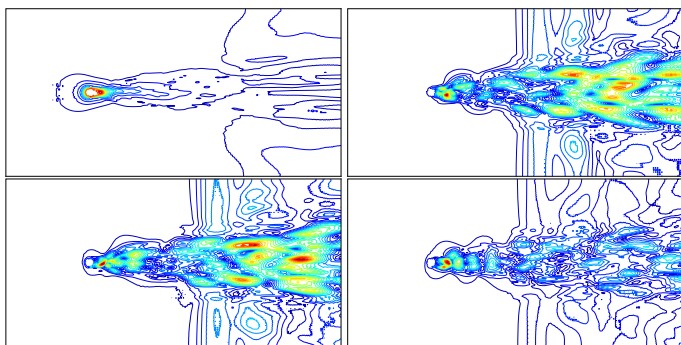


**FIGURE 6.** FIRST FOUR MODES OF THE STEADY 40000 REYNOLD'S NUMBER CASE.

about 95% of the energy content. In some cases, notably the low Reynolds number cases, the number of modes required is considerably fewer—three.

We also note that the energy decay appears roughly consistent among the four cases of mid-high Reynolds number, which suggests that this rate of decay might be representative for a

wider range of Reynolds numbers and inflow boundary conditions.

Contour plots for the absolute velocity  $\|\mathbf{v}\|$  of the first four modes in each of the *steady* cases can be seen in Figs. 4, 5 and 6. In each case, the principal mode can be seen to be “laminar” in nature, while the second and third modes provide the two phase-shifted principal oscillations directly behind the cylinder (at least, for the low and medium Reynolds number cases). Higher modes provide the more turbulent components. It stands to reason that three modes should suffice for low Reynolds number cases, where there aren't many effects other than “laminar” flow with vortex shedding.

## CONCLUSION AND FUTURE WORK

It can be concluded that for the kind of flows we simulated, POD appears to be an attractive method for constructing the RB required in ROM. In future we intend to build upon the tools / modules presented in this paper to develop computationally efficient tools that can be used on a personal computer. Although we have dealt with cylindrical shapes in this paper, the method as such is more general and can be applied to any flow. However, there are challenges associated with stability of reduced-order linearized CFD models based on POD [10] that needs to be addressed first.

The modular design of the workflow ensures that users can replace any module with their own custom module. For example, in the current work, we used OF to generate the snapshots however, we plan to replace it by our indigenous code IFEM (Isogeometric Finite Element Model [11]) developed within the FSI-WT project ([www.fsi-wt.no](http://www.fsi-wt.no)). This will enable us to utilize snapshots involving airfoils ([12] and [13]) and fluid-structure interactions ([14]) created in the past and demonstrate a wider applicability of the method. Since, the most common output format from OF and IFEM is VTK, a fileformat which is not supported by the OpenDAP server, we also need to do a trivial exercise of converting out existing database including VTK into HDF5 format.

## ACKNOWLEDGMENT

The authors acknowledge the financial support from the Norwegian Research Council and the industrial partners of FSI-WT (grant no: 216465/E20) (<http://www.fsi-wt.no>) project.

## REFERENCES

- [1] Quarteroni, A., and Rozza, G., eds., 2014. *Reduced Order Methods for Modeling and Computational Reduction*, 1<sup>st</sup> ed., Vol. 9 of *Modeling, Simulation & Applications*. Springer, Springer International Publishing Switzerland, chap. 8, pp. 235–274.

- [2] Tabib, M., Rasheed, A., and Fuchs, F., 2016. “Analyzing complex wake-terrain interactions and its implications on wind-farm performance”. *Journal of Physics Conf. Series*, **753**(032063), Oct.
- [3] Tabib, M., Rasheed, A., and Kvamsdal, T., 2015. “Investigation of the impact of wakes and stratification on the performance of an onshore wind farm”. *Energy Procedia*, **80**, pp. 302–311.
- [4] Tabib, M., Rasheed, A., and Kvamsdal, T., 2015. “LES and RANS simulation of onshore bessaker wind farm: analyzing terrain and wake effects on wind farm performance”. *Journal of Physics Conf. Series*, **625**(012032).
- [5] Siddiqui, S., Rasheed, A., Tabib, M., and Kvamsdal, T., 2016. “Numerical analysis of the nrel 5mw wind turbine: A study towards a better understanding of wake dynamics and torque generation mechanism”. *Journal of Physics Conf. Series*, **753**(032059), Oct.
- [6] Rasheed, A., Holdahl, R., Kvamsdal, T., and Åkervik, E., 2014. “A comprehensive simulation methodology for fluid-structure interaction of offshore wind turbines”. *Energy Procedia*, **53**(C), pp. 135–145.
- [7] Barbi, C., Favier, D., Maresca, C., and Telionis, D., 1986. “Vortex shedding and lock-on of a circular cylinder in oscillatory flow”. *Journal of Fluid Mechanics*, **170**, p. 527544.
- [8] NA, ed., 2017. Analysis of unsteady hydrodynamics related to vortex induced vibrations on bluff-bodies offshore structures, Submitted to 36<sup>th</sup> International Conference on Ocean, Offshore and Arctic Engineering.
- [9] Liang, C., and Papadakis, G., 2007. “Large eddy simulation of pulsating flow over a circular cylinder at subcritical reynolds number.”. *Computers and Fluids*, **36**, pp. 299–312.
- [10] Quarteroni, A., and Rozza, G., eds., 2014. *Reduced Order Methods for Modeling and Computational Reduction*, 1<sup>st</sup> ed., Vol. 9 of *Modeling, Simulation & Applications*. Springer, Springer International Publishing Switzerland, chap. 8, pp. 215–234.
- [11] Opstal, T., Fonn, E., Kvamsdal, T., Kvarving, A., Mathisen, K., Nordanger, K., Okstad, K., Rasheed, A., and Tabib, M., 2015. “Isogeometric methods for CFD and FSI-simulation of flow around turbine blades”. *Energy Procedia*, **80**, pp. 442–449.
- [12] Nordanger, K., Holdahl, R., Kvarving, A., Rasheed, A., and Kvamsdal, T., 2015. “Comparison of three isogeometric incompressible navier-stokes solvers applied to simulation of flow past a fixed NACA0012 airfoil”. *Computer Methods in Applied Mechanics and Engineering*, **284**, Feb, pp. 664–688.
- [13] Nordanger, K., Holdahl, R., Kvamsdal, T., Kvarving, A., and Rasheed, A., 2015. “Simulation of airflow past a 2D NACA0015 airfoil using an Isogeometric incompressible Navier-Stokes solver with the Spalart-Allmaras turbulence model”. *Computer Methods in Applied Mechanics and Engineering*, **290**, Feb, pp. 183–208.
- [14] Nordanger, K., Rasheed, A., Okstad, K., Kvarving, A., Holdahl, R., and Kvamsdal, T., 2016. “Numerical benchmarking of fluid-structure interaction: An isogeometric finite element approach”. *Ocean Engineering*, **124**, pp. 324–339.